Author Manuscript

Author Manuscript

Author Manuscript

Author Manuscript

HHS Public Access

Author manuscript

Nat Commun. Author manuscript; available in PMC 2014 November 28.

Published in final edited form as:

Nat Commun. ; 5: 3962. doi:10.1038/ncomms4962.

MitoNEET-Mediated Effects on Browning of White Adipose Tissue

Christine M. Kusminski[1], **Jiyoung Park**[1,&], and **Philipp E. Scherer**[1,2,*]

[1]Touchstone Diabetes Center, Department of Internal Medicine, The University of Texas Southwestern Medical Center, Dallas, Texas 75390-8549

[2]Department of Cell Biology, The University of Texas Southwestern Medical Center, Dallas, Texas 75390-8549

Abstract

MitoNEET is an outer mitochondrial membrane protein that, upon overexpression in white adipose tissue (WAT), exerts a positive impact on tissue expansion and whole-body lipid and carbohydrate homeostasis by altering mitochondrial matrix iron metabolism. Here we determine the key transcriptional events in subcutaneous WAT of mice in response to mitoNEET overexpression and a high-fat diet (HFD). Microarray analyses at key points during weight gain upon body-weight divergence with wild-type mice demonstrate that mitoNEET-enriched sWAT early on upregulates a browning signature program that limits WAT expansion in transgenic mice for a period of up to 12-weeks of HFD. This compensatory browning phenotype is subsequently lost, resulting in rapid WAT expansion and body-weight gain. Exposure to thermoneutral temperatures during HFD prompts weight gain significantly earlier. Similar WAT expansion is achieved upon infection with an adeno-associated virus expressing mitoNEET. Collectively, the mitoNEET enriched fat-pads feature a more vascularized, anti-inflammatory and less fibrotic environment.

Introduction

Obesity, now a global epidemic, is associated with a cluster of metabolic disorders such as insulin resistance, type 2 diabetes mellitus (T2DM), hyperlipidemia and hypertension [1]. Intake of high-fat diets is a key environmental factor that can profoundly contribute the development of such metabolic disorders [2–4].

Users may view, print, copy, and download text and data-mine the content in such documents, for the purposes of academic research, subject always to the full Conditions of use:http://www.nature.com/authors/editorial_policies/license.html#terms

*Corresponding author: philipp.scherer@utsouthwestern.edu, Telephone: (214) 648-8715, Fax: (214) 648-8720.
&Current address: Department of Biological Sciences, School of Life Sciences, Ulsan National Institute of Science and Technology, 50 UNIST ST., Ulsan 689-798, South Korea

Author Contributions

C.M.K. conducted all experiments and wrote the manuscript, except the portions indicated below. J.P. helped plan, perform injections and scan fat-pads in Ctl-AAV and AAV-mitoNEET experiments. P.E.S. was involved in experimental design, experiments, data analysis, and interpretation, in addition to writing of the manuscript.

Competing financial interests

The authors declare no competing financial interest.

Author Manuscript Author Manuscript Author Manuscript Author Manuscript

White adipose tissue (WAT) plays a pivotal role in maintaining whole-body energy homeostasis by storing excess energy as triglycerides (TGs) and releasing free fatty acids (FFAs) as a fuel source during energy shortage; processes crucial for proper fuel metabolism. However, during prolonged excessive caloric intake, dramatic expansion of WAT can result in a high mass of dysfunctional, inflamed and fibrotic WAT; in that state, local and whole-body glucose and lipid dysregulation prevails.

The protective effect of expandable subcutaneous fat depots during weight gain permits adequate storage of excess calories in the form of TGs to prevent ectopic lipid deposition in non-adipose cells, such as hepatocytes, myocytes and pancreatic β-cells; such lipotoxicity greatly increases the risk of insulin resistance and T2DM [5,6]. Therefore, understanding the mechanisms by which subcutaneous WAT (sWAT) expandability is regulated, with particular emphasis on how to sustain *healthy* non-fibrotic, non-inflamed sWAT expansion during excess nutrient intake, in addition to pushing the maximum capacity for sWAT expansion to higher limits to prevent lipotoxic insults, is of great importance.

Under physiological conditions, lipid and glucose homeostasis is largely dependent on fully functional mitochondria; the *cellular power houses* that generate ATP to sustain cellular function. Mitochondrial dysfunction on the other hand, is emerging as a central contributory factor in the development insulin resistance and T2DM [7–12]. In terms of WAT, malfunction of mitochondrial activity can have a profound effect upon white adipocyte physiology [13]. Adipocyte mitochondria provide key intermediates for TG synthesis and are critical for lipogenesis; similarly, increased mitochondrial biogenesis is vital during the adipogenic process [14,15]. In addition to this, WAT mitochondria are pertinent for β-oxidation of liberated fatty acids during lipolysis; a key source of ATP to meet the energy demands during starvation [13]. Collectively, any mitochondrial disruption in adipocyte pathways contributes vastly to the development of insulin resistance [13,14,16,17].

We previously generated a mouse model in which the amount of mitochondrial activity in adipocytes could be altered based on the properties of the outer mitochondrial membrane protein mitoNEET [18]. By overexpressing mitoNEET in adipocytes and combining the added metabolic challenge of a leptin-deficient *ob/ob* background, despite the prevalence of chronic obesity, mice exhibited system-wide improvements in insulin sensitivity; this provided a model of a “metabolically healthy” obese state, with minimal lipotoxicity [18]. MitoNEET achieves these remarkable and potent effects on WAT expansion by modulating mitochondrial iron metabolism [18].

Here, to divert away from the severity of an *ob/ob* challenge and thus activation of secondary compensatory mechanisms, we examine the initial mechanisms by which mitoNEET triggers WAT expansion during high-fat diet (HFD) feeding. In particular, we identify that mitoNEET initiates a prominent transcriptional “browning” program during HFD exposure. The transgenic animals maintain the same weight as their wildtype littermates up to a point when this transcriptional browning program fails to be maintained at a high level. At that point, WAT expandability capacity is enhanced in transgenic mice, prompting an immediate increase in body-weight gain. Nevertheless, healthy WAT

Author Manuscript Author Manuscript Author Manuscript Author Manuscript

expansion prevails, with less HFD-driven inflammation and fibrosis evident with the local increase in mitoNEET, which ultimately results in an improved systemic metabolic profile.

Results

MitoNEET alters the browning signature of WAT

We recently reported that adipose-specific mitoNEET transgenic mice (*MitoN-Tg* mice) undergo massive, yet "healthy" WAT expansion of the subcutaneous fat-depot when metabolically challenged in a leptin-deficient *ob/ob* background [18]. While the *ob/ob* cross presents a severe metabolic challenge that rapidly elicits secondary compensatory mechanisms in WAT, we wanted to investigate mitoNEET action in a less severe metabolic setting to establish the initial mitoNEET-induced effects that occur prior to massive WAT expansion. With this in mind, HFD feeding allows us to assess the gradual increase in body-weight gain and potentially capture any key transcriptional or signaling events in which mitoNEET activates WAT expansion.

Under chow-fed conditions, no marked differences in body-weight gain were apparent between wild-type (WT) mice and *MitoN-Tg* mice (Fig. 1a). We subsequently challenged mice with a HFD (60% kcal fat). While no significant differences in body-weight gain were evident during the initial 12-weeks of HFD feeding (Fig. 1b; arrow a), body-weights reproducibly began to diverge around 13-weeks of HFD feeding, which gradually became more apparent by week-15 (Fig. 1b; arrow b). In light of this, we wanted to identify the critical determinants triggered by mitoNEET that initiate WAT expansion at this stage. We therefore performed microarray analyses on sWAT tissues specifically at week-12 of HFD feeding (prior to body-weight divergence) and at week-15 of HFD feeding (post body-weight divergence). Table 1 highlights key genes markedly *upregulated* in *MitoN-Tg* sWAT between week-12 and week-15 of HFD feeding, which are either unaltered or oppositely regulated in WT sWAT during this timeframe; such genes include *11βHSD1*, *Erg1*, *Sema5a*, *Col16a1* and *Rarres2* (Chemerin). Under similar conditions, Table 2 provides genes significantly *downregulated* between week-12 and week-15 of HFD feeding in *MitoN-Tg* sWAT. Interestingly, analysis revealed a marked reduction in the transcriptional signature program that drives the "beiging" phenotype of sWAT, with key brown adipose tissue (BAT)-indicator genes including *Otop1*, *Cidea*, *Ucp1*, *Cox7a1* and *Cox8b* being reduced (Table 2).

In addition, a reduction in mitochondrial β-oxidation pathways was evident; target genes downregulated at various steps of β-oxidation entailed *Acadvl*, *Cyp2e1*, *Cpt2*, *Acaa2*, *Slc25a20*, *Aco2*, *Decr1* and *Etfb* (Table 2). With respect to browning, qPCR analyses confirmed the reduction in BAT-selective genes (*Otop1*, *Cidea*, *Cox7a1* and *Prdm16*) between week-12 HFD *versus* week-15 HFD in *MitoN-Tg* sWAT (Fig. 1c). Surprisingly, when comparing WT sWAT *versus MitoN-Tg* sWAT at week-12 of HFD, a significant *increase* in factors mediating browning of WAT was apparent in mitoNEET transgenics (Fig. 1c). Of note, no marked differences in these browning genes were observed between WT sWAT and *MitoN-Tg* sWAT under chow-fed conditions (Supplementary Fig. 1a). To explore this browning aspect further, we examined the differential regulation pattern of two widely established BAT-indicator genes, *Pgc1α* and *Ucp1* [19–22]. Under chow-fed conditions

Author Manuscript Author Manuscript Author Manuscript Author Manuscript

and 2-weeks of acute HFD feeding, *Pgc1α* message levels are significantly upregulated in *MitoN-Tg* sWAT (Fig. 1d). However, both *Pgc1α* and *Ucp1* are profoundly upregulated in *MitoN-Tg* sWAT at 12-weeks HFD feeding (Fig. 1d). In contrast, by week-15 of HFD, both *Pgc1α* and *Ucp1* are significantly downregulated in transgenic sWAT; this downregulation persists even up to 24-weeks HFD feeding (Fig. 1d). Consistent with the increase in *Pgc1α* expression under chow-fed conditions, we observed an upregulation in mitochondrial protein expression in *MitoN-Tg* sWAT, in particular complex I and complex IV of the mitochondrial ETC (Fig. 1e); such upregulation was specific for the subcutaneous fat-pad, the primary site of mitoNEET overexpression. We previously reported *MitoN-Tg* sWAT harbors mitochondria that are functionally compromised in oxidative respiration [18]. Here, the upregulation in mitochondrial protein is likely a Pgc1α-dependent compensatory increase in mitochondrial biogenesis. The patterns of differential Pgc1α and Ucp1 regulation in the transgenic sWAT were also evident at the protein level, as seen by western blot and immunohistochemical analyses (Figs 1f and 1g, respectively).

Thermoneutrality enhances WAT expansion in *MitoN-Tg* mice

The profound upregulation in the browning program within *MitoN-Tg* sWAT during 12-weeks of HFD feeding (Fig. 1c and 1d) may serve as a key contributory factor that prevents full activation of WAT expansion in *MitoN-Tg* mice and therefore, could partially explain the initial lack of difference in body-weight gain between WT and *MitoN-Tg* mice up to 12-weeks HFD feeding (Fig. 1b). To test this hypothesis, we metabolically challenged mice with HFD feeding under thermoneutral conditions, with the prediction that the euthermic conditions would minimize the effects of the large upregulation in browning in *MitoN-Tg* sWAT during the early stages of HFD feeding and thus a difference in body-weight would become apparent within an earlier timeframe of HFD feeding. In particular, the thermoneutral zone in mice is approximately 30°C. Such temperatures allow the lowest rate of energy expenditure required to maintain body temperature to be sustained [23–25]. Indeed, upon HFD feeding under thermoneutrality, *MitoN-Tg* mice gained significantly more body-weight than WT mice, with body-weight differences starting to diverge at the 8-week time-point already (Fig. 2a); indicating that *MitoN-Tg* mice display an earlier activation of WAT expansion through a reduction in the browning program. Interestingly, despite *MitoN-Tg* mice displaying almost twice the size in body-weight when compared to their WT littermates when kept under these thermoneutral conditions, thus receiving twice the glucose load, glucose clearance is fully preserved (Fig. 2b); a phenomenon also observed in *MitoN-Tg-ob/ob* mice [18].

In contrast to thermoneutrality, we performed cold tolerance tests to assess any potential defects in thermogenesis in *MitoN-Tg* mice either under chow-fed conditions or with HFD feeding. However, we noted no significant differences in body-temperature between WT mice and *MitoN-Tg* mice either in an acute setting of cold-exposure post chow-diet feeding, or a more chronic setting of cold-exposure post HFD feeding (Supplementary Fig. 1b).

MitoNEET-induced WAT expansion promotes insulin sensitivity

To evaluate the extent to which mitoNEET impacts sWAT expansion, we sustained a more prolonged metabolic challenge of chronic HFD feeding. Interestingly, *MitoN-Tg* mice

Author Manuscript Author Manuscript Author Manuscript Author Manuscript

sustain almost twice the body-weight in comparison to their WT littermates (WT: 48.3 ± 1.3 g; *MitoN-Tg*: 82.0 ± 2.0 g, Student's *t*-test $P < 0.001$) (Fig. 3a). Visually, micro-CT scans confirmed this gross AT expansion in *MitoN-Tg* mice following prolonged HFD feeding (Fig. 3b). Quantitatively, both sWAT and gWAT fat-pads are significantly larger in adipose tissue (AT) volume (Fig. 3c), despite previously observing a marked reduction in gWAT fat-pad size under chow-fed conditions [18].

An initial evaluation revealed no significant differences in insulin-sensitivity between WT mice and *MitoN-Tg* mice under chow-fed conditions (Fig. 3d), or upon exposure to a HFD challenge for up to 12-weeks (Fig. 3e) (prior to the divergence in body-weight gain (Fig. 1b; arrow a). However, a significant difference in glucose tolerance only became apparent once *MitoN-Tg* mice were exposed to HFD following a period of more than 15-weeks. In particular, despite weighing more than their WT littermates, *MitoN-Tg* mice exhibit a marked improvement in glucose-tolerance, even when glucose load is adjusted to total body-weight (Fig. 3f); therefore, obese *MitoN-Tg* mice very effectively remove considerably more exogenous glucose from circulation than their WT littermates. In addition, chronic HFD-fed *MitoN-Tg* mice have the capacity to preserve their β-3 adrenergic agonist sensitivity. Following β-3 stimulation, *MitoN-Tg* mice exhibit significantly higher systemic levels of glycerol and FFAs (Fig. 3g). However, the FFA levels are vastly substoichiometric, an indication of substantial FFA re-esterification to TG, which is reflected by AT expansion.

Hormone-sensitive lipase (HSL) is a key enzyme mediating the activation of lipolysis [26]. To further address the enhanced β-3 adrenergic agonist sensitivity in transgenic mice, we examined HSL phosphorylation following β-3 stimulation. A marked increase in phospho-HSL (p-HSL) was evident in *MitoN-Tg* sWAT, whereas no significant differences between *MitoN-Tg* gWAT and WT gWAT were apparent (Fig. 3h); the latter pinpoints the specificity of enhanced β-3 adrenergic agonist sensitivity to the mitoNEET-enriched sWAT. Gene expression analysis further corroborated an association between increased mitoNEET levels and β-3 adrenergic signaling pathways, as β-adrenergic receptor 1 (*β-AR1*), *β-AR2* and *β-AR3*, in addition to HSL expression levels were shown to be significantly upregulated in *MitoN-Tg* sWAT under chow-fed conditions. A similar upregulation was also observed in 12-week, 15-week and >24-weeks high-fat diet (HFD) feeding studies (Figure 3i).

In line with improved whole-body insulin sensitivity in a state of chronic HFD feeding, histology further revealed minimal hepatic lipid accumulation in *MitoN-Tg* mice when compared with WT livers (Fig. 3j); collectively, accentuating that AT expansion minimizes obesity-induced hepatic steatosis and preserves insulin sensitivity. Finally, we previously reported some degree of mitoNEET overexpression was evident in BAT; albeit the subcutaneous fat-pad predominantly harbors the bulk of mitoNEET overexpression [18]. We also noted that under chow-fed conditions, *MitoN-Tg* BAT is significantly larger in size when compared with WT BAT [18]. In light of this, we assessed BAT adipocyte size and observed that *MitoN-Tg* BAT harbors more lipid-droplets under chow-fed conditions; moreover, HFD feeding appears to result in the formation of even larger adipocytes in *MitoN-Tg* BAT (Fig. 3k). Collectively, this suggests that while *MitoN-Tg* BAT is overall larger in size and harbors more lipid-droplets under chow feeding, HFD feeding does not

Author Manuscript Author Manuscript Author Manuscript Author Manuscript

promote hyperplastic expansion in *MitoN-Tg* BAT, as typically observed in *MitoN-Tg* sWAT.

MitoNEET favors M2 macrophage anti-inflammatory phenotypes

Under chronic HFD-fed conditions, AT histology in *MitoN-Tg* sWAT appeared comparable to that of a healthy mouse on chow diet, with normal adipocyte-cell size in comparison with enlarged hypertrophic adipocytes observed in WT sWAT under the same HFD conditions (Fig. 4a). To some extent, these differences were also preserved between WT gWAT and *MitoN-Tg* gWAT (Fig. 4a). Of note, we demonstrate that expression of the mitoNEET transgene is restricted primarily to adipocytes with minimal expression in other cell-types, such as macrophages; with the highest level of mitoNEET expression observed in sWAT relative to gWAT and isolated macrophages (Fig. 4b; left). Moreover, we further assessed *endogenous* mitoNEET expression levels in adipocytes and the stromal vascular fraction (SVF) of both sWAT *versus* gWAT fat-depots. We observed that the highest levels of mitoNEET are expressed in sWAT adipocytes, when compared with gWAT adipocytes (Fig. 4b; right). Furthermore, both sWAT and gWAT adipocyte fractions contained higher levels of mitoNEET relative to SVF derived from either sWAT or gWAT fat-pads (Fig. 4b; right). Collectively, this demonstrates that endogenous mitoNEET levels are considerably higher in adipocytes than cells of the SVF (the latter containing cells such as preadipocytes, macrophages and endothelial cells); this may reflect the physiological roles that mitoNEET plays in each of these cell-types.

During HFD feeding, obesity initiates a state of low-grade inflammation and fibrosis, which ultimately pre-disposes to the progression to insulin resistance and T2DM [27–29]. In particular, obese AT harbors a high degree of infiltrating macrophages, typically termed *adipose tissue macrophages* (ΦATMs); such ΦATMs play an instrumental role in initiating a heightened state of chronic inflammation and associated metabolic dysfunctions [30–32]. More specifically, the *type* of ΦATMs within AT contributes to the type of AT expansion during the progression of obesity. Several studies have demonstrated that ΦATMs derived from lean mice express markers of M2 or “alternatively activated” macrophages; conversely, obese states harbor a reduction in M2 markers, with concomitant increases in M1 or “classically activated” macrophages [33]. Generally, an influx of M2 macrophages into AT is considered an anti-inflammatory characteristic that is associated with beneficial processes, such as angiogenesis and wound repair [33]. In contrast, M1 macrophage polarization is considered more pro-inflammatory and is associated with metabolic dysfunction and tissue destruction [33]. In light of this, we wanted to first establish whether mitoNEET-induced expansion of AT during HFD-feeding promotes an influx of ΦATMs and secondly if so, which *type* of macrophages infiltrate AT-enriched with mitoNEET. Total macrophage marker gene expression levels, as determined *F4/80*$^{+}$ and *Cd45*, were significantly lower in *MitoN-Tg* sWAT, when compared with WT sWAT (Fig. 4c). Consistent with this, Mac2 immunohistochemistry revealed considerably more macrophage staining in HFD-fed WT sWAT; displaying an increased presence of “crown-like” structures (macrophages encircled around adipocytes) (Fig. 4d). In contrast, very few of these crown-like structures were observed in HFD-fed *MitoN-Tg* sWAT (Fig. 4d). Similarly, WT gWAT also harbored more macrophages and crown-like structures in comparison to *MitoN-Tg* gWAT (Fig. 4d). When

Author Manuscript Author Manuscript Author Manuscript Author Manuscript

examining the type of macrophages residing within HFD-induced obese AT, *MitoN-Tg* sWAT was shown to express significantly higher levels of the anti-inflammatory M2 macrophage markers *Cd206*, *Cd301* and *Cd163* (when normalized to *F4/80*$^{+}$ expression levels), in comparison to WT sWAT (Fig. 4e). Conversely, from a pro-inflammatory angle, *MitoN-Tg* sWAT was shown to express markedly less of the pro-inflammatory M1 macrophage markers MCP-1 and IL-6, when compared with WT sWAT (Fig. 4f). Finally, T-cells have the capacity to infiltrate 'inflamed' obese AT and resolve some of that inflammation [34–39]. In light of this, *MitoN-Tg* sWAT was shown to express significantly higher levels of the T-cell markers forkhead box P3 (*FoxP3*) and the transcription factor T-bet (upon normalization to *F4/80*$^{+}$ expression levels), when compared with WT sWAT (Fig. 4g). Previous studies have documented that WAT resident FoxP3-expressing regulatory T cells exhibit the capacity to reverse obesity-linked insulin resistance and decrease inflammation [40,41]. Moreover mice deficient in the transcription factor responsible for the development of T helper cells, *T-bet*, while developing an obesogenic phenotype, exhibit hallmarks of an unhealthy metabolic profile [42]. Taken together, these studies suggest that during HFD-induced WAT expansion, *MitoN-Tg* sWAT harbors immune cells that promote an anti-inflammatory environment suitable for healthy WAT expansion.

MitoNEET-driven healthy WAT expansion ameliorates fibrosis

Given that we observe healthy AT expansion in *MitoN-Tg* sWAT following chronic HFD challenge, we subsequently assessed whether the overexpression of mitoNEET alters the vasculature. Gene expression profiling revealed that several endothelial markers are significantly upregulated in *MitoN-Tg* sWAT, when compared with WT sWAT; namely, *Vegf*, *Vegf-R1*, *Tie2*, *Elastin*, *Cd31* and *Flt-1* (Fig. 5a). Furthermore, trichrome staining of sWAT and gWAT fat-pads revealed that HFD challenged *MitoN-Tg* sWAT exhibits markedly less fibrosis in comparison to WT sWAT (Fig. 5b); again reflecting the healthy state of AT expansion under extreme metabolic challenges. Such differences in fibrotic WAT were further exacerbated in the gonadal fat-pads between the WT and transgenic groups (Fig. 5b). We further observed significant decreases in *Col3α1* and *Col1α1* gene expression levels in HFD-fed *MitoN-Tg* sWAT, when compared with WT sWAT (Fig. 5c). Finally, we previously observed that gene expression markers of fatty-acid (FA)-uptake, adipogenesis and glucose-uptake are upregulated in *MitoN-Tg* sWAT under chow-fed conditions [18]. Similarly, *Fas*, *Fasn*, *Pparγ*, *Glut4* and *Pepck* gene expression levels were markedly increased in *MitoN-Tg* sWAT, when compared with WT sWAT (Fig. 5d).

Adenoviral overexpression of mitoNEET promotes WAT expansion

While the constitutive *aP2*-driven transgene expression has proven to be a powerful tool to investigate the effects of mitoNEET overexpression, we subsequently intended to independently confirm our current findings. We therefore utilized an additional approach. To pinpoint the specificity and capacity of mitoNEET to expand AT during times of surplus caloric-intake, we generated an adeno-associated virus carrying the mitoNEET cDNA (MitoN-AAV8) and hypothesized that upon viral delivery, a larger fat-pad would be emerge. To effectively infect adipocytes, we opted to utilize AAV serotype 8. We injected MitoN-AAV8 into the right sWAT fat-pad of WT mice and, as an internal control we injected a control virus (Ctl-AAV8) into the left sWAT fat-pad, which does not over-express

Author Manuscript Author Manuscript Author Manuscript Author Manuscript

mitoNEET (Fig. 6a). Both viruses contain a functional green fluorescent protein that allowed us to monitor the infection efficiency. Interestingly, the fat-pad enriched with mitoNEET was markedly larger visually and in weight within four weeks post infection, despite both experimental and control fat-pads being successfully infected with virus, as evident by the GFP signal (Fig. 6b). No apparent differences were observed for non-infected gWAT control fat-pads (Fig. 6b). H&E staining of sWAT fat-pads revealed no apparent differences in adipocyte size between Ctl-AAV8 sWAT and MitoN-AAV8 sWAT (Fig. 6c). Given that the MitoN-AAV8 fat-pad is larger in size (Fig. 6b), and the average adipocyte size appears comparable, we conclude that an increase in adipogenesis is the likely explanation for the increase fat pad size. This is overall consistent with the genetic mouse model of chronic overexpression. Finally, upon examination of WAT inflammation, we observed a significant reduction in gene expression levels of the pro-inflammatory marker TNFα in MitoN-AAV8 sWAT, when compared with Ctl-AAV8 sWAT; concomitant with a moderate increase in levels of the anti-inflammatory M2 macrophage marker, Cd163 expression (Fig. 6d). Collectively suggesting that mitoNEET may further promote a non-inflamed environment for WAT expansion.

Discussion

Here, we have embarked on a detailed temporal analysis of the effects of mitoNEET overexpression in WAT. We find that upon exposure to HFD, mitoNEET as previously reported is likely to reduce the oxidative capacity of sWAT. However, as a compensatory mechanism, we observe that sWAT induces a significant “beiging” program that maintains the body weight of the transgenic animals. This compensatory increase is abruptly lost after approximately 12 weeks of HFD feeding, and it is at that time that weight differences start to become rapidly apparent. We can shift this period of weight gain by neutralizing the beiging effects of sWAT under thermoneutral conditions. During the expansion phase, minimal HFD-induced WAT inflammation prevails, with mitoNEET promoting anti-inflammatory M2 macrophages to reside within WAT, as opposed to pro-inflammatory M1 macrophages that typically reside within inflamed obese WAT. In addition, mitoNEET ameliorates HFD-driven fibrosis and promotes angiogenesis; the latter helping to sustain a fully vascularized fat-pad during the expansion process. Collectively, abundant local mitoNEET levels in adipose tissue result in profound improvements in whole-body systemic carbohydrate and lipid homeostasis, particularly with respect to preservation of insulin sensitivity, minimal obesity-induced hepatic steatosis and enhanced β-3 adrenergic agonist sensitivity. Finally, the mitoNEET-induced WAT expansion *in vivo* can be recapitulated using adenoviral-mediated injection of mitoNEET specifically into the subcutaneous fat-pad, further pinpointing the primary mitoNEET-driven WAT expansion.

White and brown adipocytes exert opposing functions in energy balance regulation [43]. White adipocytes store surplus energy in lipid droplets; conversely brown adipocytes dissipate energy through non-shivering thermogenesis and may ameliorate diet-induced obesity through such an energy wasting mechanism [23,44,45]. During the time spectra of HFD feeding, MitoN-Tg mice exhibit a unique differential pattern of beige AT-indicator gene expression during the progressive stages of sWAT expansion. In particular, *Pgc1α* and *Ucp1* are vastly *upregulated* up to, and at, the 12-week stage of HFD feeding. Then, surprisingly

Author Manuscript Author Manuscript Author Manuscript Author Manuscript

by the 15-week stage of HFD feeding, both *Pgc1α* and *Ucp1* are significantly *downregulated* in transgenic sWAT. We previously identified that an overexpression of mitoNEET in WAT compromises mitochondrial β-oxidation by lowering mitochondrial matrix iron content [18]; such effects may result in insufficient iron-sulfur cluster import into the matrix, thus hindering mitochondrial respiratory complex formation and efficient electron transfer through the electron transport chain (ETC). HFD-induced activation of the browning program in transgenic mice at week-12 suggests a compensatory mechanism whereby mitochondria divert the excess energy from surplus dietary lipids away from an impaired ETC to utilize alternate avenues that enable energy dissipation as heat via Ucp1-dependent thermogenesis. Consistent with this notion, no difference in body-weight is evident between WT mice and *MitoN-Tg* mice up to 12-weeks of HFD feeding, therefore a vast upregulation in browning and thermogenesis could help cope with a large lipid influx into transgenic sWAT, as transgenics are known to exhibit an increase rate in lipid-uptake [18]. Indeed, murine studies have demonstrated that overexpression of Ucp1 in WAT [15] and preadipocytes during adipocyte differentiation results in reduced accumulation of lipids [46]. Finally, the profound mitoNEET-induced downregulation in browning signature genes at week-15 HFD in transgenic sWAT likely activates unrestricted WAT expansion, which is mirrored by a divergence in body-weight gain, with transgenic mice now displaying a marked increase in body-weight gain.

Thermoneutrality refers to the temperature at which the energy expenditure required to maintain body temperature is lowest [23,25]. Mice achieve thermoneutrality at approximately 30°C. However, laboratory mice are typically housed at “room temperature”, generally 18°C–22°C and are therefore, under chronic thermal stress and must increase their metabolism by approximately 50% [24]. To potentially counteract the upregulation in browning events that occur prior and up to the 12-week stage of HFD feeding that may hinder full activation of WAT expansion processes in *MitoN-Tg* mice, we applied the same metabolic challenge albeit under thermoneutral conditions. As expected, *MitoN-Tg* mice exhibit a steeper curve in body-weight gain under thermoneutral conditions than under room temperature, as observed by body-weight differences becoming apparent at 8-weeks HFD feeding, rather than 15-weeks HFD feeding, respectively; implicating earlier activation of WAT expansion mechanisms through a reduction in the browning program. In fact under HFD fed thermoneutral conditions, here we report the heaviest non-*ob/ob* mouse, which reached 114.2 g in body-weight. Certainly, other studies have documented that during HFD feeding, Ucp1-deficient mice fail to become obese under laboratory conditions of 18°C–22°C [47], however become obese, although not remotely to the same degree as *MitoN-Tg* mice, when maintained under thermoneutrality [48].

Healthy WAT expansion has the capacity to prevent diet-induced lipotoxicity and the development of insulin resistance [5]. More specifically, each standard deviation increase in sWAT mass decreases the chances of insulin resistance by 48%; conversely, each standard deviation increase in visceral AT mass increases the chances of insulin resistance by 80% [49]. *MitoN-Tg* mice undergo gross, yet hyperplastic sWAT expansion during chronic HFD feeding, which protects them from lipotoxicity and effectively preserves insulin sensitivity. Indeed, this metabolically healthy yet obese (MHO) paradox translates well to clinical

Author Manuscript Author Manuscript Author Manuscript Author Manuscript

findings, whereby unique subsets of morbidly obese patients are protected against obesity-related metabolic disturbances due to their capability to expand sWAT [50–52]. Despite a clinical awareness of MHO patients, which account for 20–30% of the obese population [52], there is only a rudimentary understanding of factors and mechanisms underlying this phenotype and further, underscores the need to identify and understand factors underlying the protective profile in MHO patients. Here, we identify a mouse model that mimics MHO patients; such that by altering the levels of a mitochondrial protein mitoNEET specifically in sWAT, we promote HFD-induced sWAT expansion and very effectively preserve carbohydrate homeostasis. With regards to examining mechanisms of sWAT expansion, our laboratory recently generated an inducible mouse model of permanently labeling mature adipocytes blue, which we coined the "AdipoChaser" mouse [53]. Utilizing this unique mouse model, we identified that the majority of sWAT adipogenesis occurs early in life between embryonic days 14 and 18, and that later in life, with the addition of HFD feeding, sWAT expands through hypertrophic growth of adipocytes [53]. While in this current study we demonstrate that mitoNEET may promote HFD-induced hyperplastic sWAT expansion, as judged by smaller sWAT adipocytes upon metabolic challenge, future studies examining whether mitoNEET has the capacity to drive diet-induced adipogenesis in sWAT during the later stages in life, a phenomenon not typically observed in expanding sWAT, should prove illuminating.

HFD-induced obesity is linked to a low-grade chronic pro-inflammatory state, in which macrophage infiltrate and reside within WAT and polarize from an anti-inflammatory M2 phenotype towards a pro-inflammatory M1 phenotype; this serves as a key contributory factor in the development of insulin resistance and T2DM [27,32,54]. Following HFD feeding, *MitoN-Tg* sWAT expresses high levels of the anti-inflammatory M2 macrophage markers and conversely, low levels of pro-inflammatory M1 macrophage markers; collectively indicating that mitoNEET promotes healthy non-inflamed sWAT expansion. Consistently from a clinical perspective, Karelis and colleagues noted that a favorable inflammation status was evident in the protective profile of obese MHO individuals [50].

Angiogenesis is the process of new vasculature formation and is critical in providing growing and proliferating adipocytes with vascular supply during WAT expansion [29,55]; a limited vascular source to expanding WAT can thus impede its maximal expandability capacity. The initiation of angiogenesis comprises of the proliferation of endothelial cells and is mediated by the growth factor Vegf-A, acting through its receptor, Vegf-R2 [56,57]. HFD-induced expanding *MitoN-Tg* sWAT possesses a high maximal expandability limit, particularly under thermoneutrality whereby we observe a 114.2 g non-*ob/ob* mouse. This is complemented with a significant increase in VEGF expression in *MitoN-Tg* sWAT, suggesting that proliferating adipocytes enriched with mitoNEET emanate angiogenic signals that trigger and ensue adequate vasculature formation and a robust blood supply that complements the rapidly expanding sWAT. Finally in addition angiogenesis, for healthy sWAT to progress, the extracellular matrix (ECM) surrounding adipocytes, which principally consists of collagen, must be remodeled [29]. If ECM remodeling does not occur, an upregulation of ECM components occurs, at least in part as a response to the hypoxic conditions that prevail and lead to an upregulation of Hif1α, resulting in severe

Author Manuscript Author Manuscript Author Manuscript Author Manuscript

fibrosis [29,58,59], a key feature in pathological sWAT expansion. Here, we observe that *MitoN-Tg* sWAT harbors markedly less HFD-induced fibrosis and lower collagen expression; collectively confirming healthy, non-inflamed, non-fibrotic, highly vascularized models of sWAT expansion that ultimately preserve insulin sensitivity during HFD feeding.

In summary, here we identify that during the initial stages of a HFD challenge, mitoNEET-enriched sWAT upregulates a browning program that appears to dissipate surplus dietary energy for a period of up to 12-weeks. Shortly preceding this timeframe, mitoNEET then loses the ability to maintain this BAT program in sWAT; this triggers WAT expansion, which is paralleled by sudden increase in body-weight gain in the transgenic mice. It is not clear why the adipocytes lose their ability maintain their BAT program after 12 weeks on the HFD. This is driven by the number of weeks on the HFD, not by age of the mice. It is tempting to speculate that this may have something to do with the “crisis” that occurs around 12–14 weeks into HFD feeding reported by Obin and colleagues [60]. This “crisis” reflects widespread adipocyte death followed by re-emergence of new adipocytes that may differ in their differentiation program and now no longer offer the compensatory upregulation of the BAT transcriptional program.

Methods

Animals

All animal experimental protocols were approved by the Institutional Animal Care and Use Committee of University of Texas Southwestern Medical Center at Dallas. Adipose tissue specific mitoNEET transgenic mice were generated by subcloning the mitoNEET gene into a plasmid containing the 5.4-kb *aP2*-promoter and a conventional 3′ untranslated region [61]. Following linearization, the construct was injected into FVB-derived blastocysts. Transgene-positive offspring were genotyped using PCR with the primer set: 5′-GGACCTCTGATCATCAAGA and 5′-GGAGACAATGGTTGTCAAC. All overexpression experiments were performed in a pure FVB background. All experiments were conducted using littermate-controlled male or female mice. All HFD experiments were initiated at approximately 6–12-weeks of age.

Systemic tests and blood chemistry

For the OGTT, mice were fasted for 3 h prior to administration of glucose (2.5 g kg^{-1} body-weight by gastric gavage). At the indicated time-points, venous blood samples were collected in heparin-coated capillary tubes from the tail-vein. Glucose levels were measured using an oxidase-peroxidase assay (Sigma-Aldrich). Mice did not have access to food throughout the experiment. For the β_3-adrenergic receptor-agonist sensitivity test, tail-vein serum samples were obtained before and 5-, 15-, and 60 min following intraperitoneal injection of 1 mg kg^{-1} CL 316,243 (Sigma-Aldrich, St. Louis, MO). Insulin and adiponectin levels were measured using commercial ELISA kits (Millipore Linco Research, St. Charles, MO). Glycerol and glucose levels were determined using a free glycerol reagent and an oxidase-peroxidase assay, respectively (Sigma-Aldrich). TG levels and cholesterol levels were measured using Infinity reagents (Thermo Fisher Scientific, Waltham, MA). FFA levels were measured with a NEFA-HR(2) kit (Wako).

Author Manuscript Author Manuscript Author Manuscript Author Manuscript

Cold exposure

For cold exposure experiments, ~12-week old WT mice and *MitoN-Tg* mice were kept in individual cages and maintained on chow-diet for 3 d prior to cold exposure. During cold exposure, mice were fasted (4 h) prior to being housed in a cold cabinet (6°C) with either no food (an acute setting of 6 h) or free access to food (chronic setting of 2-weeks HFD) and water.

Computed topography

For *in vivo* micro-CT scanning, mice were anesthetized with 1% isoflurane inhalation and a whole-body scan was performed at a resolution of 93 μm (80 kV, 450 μA and 100 ms integration time) using an eXplore Locus Micro-CT scanner (GE Healthcare, Little Chalfont, Buckinghamshire, UK). The micro-CT scanner was calibrated according to protocols provided by the manufacturer. Each scan took approximately 10 min and the mice showed no sign of discomfort during the procedure. The images obtained were analyzed using Microview software (GE Healthcare). Using the Microview software, WAT quantification was assessed from the base of the lungs to the distal side of the hip joint. For determination of total AT volume, histogram analysis of CT images showed that voxels with CT values between -380 and -120 Hounsfield units (H.U) are defined as AT. The abdominal muscular wall was used as the differentiation line to separate sWAT from gWAT. Then gWAT was analyzed by assessing the fat content within the peritoneal cavity using the clearly visible peritoneum as guidance. The sWAT was obtained by subtracting gWAT from total body-fat. Color-coded 3D-images of sWAT and gWAT were generated from the histograms using a volume-rendering tool (Microview software).

Quantitative real-time PCR and microarray

Tissues were excised from mice and snap-frozen in liquid nitrogen. Total RNA was isolated following tissue homogenization in Trizol (Invitrogen, Carlsbad, CA) using a TissueLyser (Qiagen, Valenica, CA), then isolated using an RNeasy RNA extraction kit (Qiagen). The quality and quantity of the RNA was determined by absorbance at 260/280 nm. cDNA was prepared by reverse transcribing 1 ug of RNA with SuperScript III reverse transcriptase and oligo$(dT)_{20}$ (Invitrogen). Table 3 highlights the primer sets that were used for quantitative RT-PCR. Results were calculated using the threshold cycle method [62], with β-actin used for normalization.

Immunoblotting

Frozen tissue was homogenized using a TissueLyser (Qiagen) in TNET buffer (50 mM Tris-HCl [pH 7.6], 150 mM NaCl, 5 mM EDTA, phosphatase inhibitors [Sigma Aldrich] and protease inhibitors [38]), followed by low centrifugation and removal of any adipose-layer present. Following addition of Triton X-100 to a final concentration of 1%, protein concentrations were determined using a bicinchoninic acid assay (BCA) kit (Pierce). Proteins were resolved on either a 4–12% bis-Tris gel (Invitrogen) or a 10–20% Tricine gel (Invitrogen) and transferred to a polyvinylidene difluoride membrane (Millipore) or a nitrocellulose membrane (Protran, Whatman GmbH, Germany), respectively. A polyclonal antibody for Ucp1 was used (1: 250; Abcam, Cambridge, MA). Polyclonal antibodies for

Author Manuscript Author Manuscript Author Manuscript Author Manuscript

total-HSL and p-HSL (Ser-660) were utilized (1:1000; Cell Signaling Technology, Inc., MA). A monoclonal MitoProfile Total OXPHOS Rodent Antibody Cocktail was also used (1:1000; MitoSciences, Cambridge, MA). Primary antibodies were detected using secondary immunoglobulin Gs labeled with infrared dyes emitting at 700 and 800 nm (1:5000; Li-Cor Bioscience, Lincoln, NB) then visualized on a Li-Cor Odyssey infrared scanner (Li-Cor Bioscience). The scanned data were analyzed using Odyssey Version 2.1 software (Li-Cor Bioscience). Full-length scans of immunoblots are shown in Supplementary Figure 2.

Histology and immunohistochemistry (IHC)

The relevant fat-pads or liver tissues were excised and fixed in 10% PBS-buffered formalin for 24 h. Following paraffin embedding and sectioning (5 μm), tissues were stained with H&E or a Masson's Trichrome stain. For IHC, paraffin-embedded sections were stained using polyclonal anti-Ucp1 antibodies (1:250; Abcam, Cambridge, MA) or monoclonal anti-Mac2 antibodies (1:250; CEDARLANE Laboratories USA Inc., Burlington, NC).

AAV experiments

WT mice were injected with Ctl-AAV8 or MitoN-AAV8 (5×10^{11} PFU) (Vector Biolabs, PA) directly into the left and right fat-pads, respectively. Following HFD-feeding (4-weeks), fat-pads were monitored for GFP signal using a fluorescence scanner (IVIS, Caliper Life Sciences, MA).

Isolation of mouse peritoneal macrophages

Peritoneal macrophages were collected from 12-week-old male FVB WT and *MitoN-Tg* mice by peritoneal lavage with 10 ml of PBS, centrifuged at 1,000 rpm for 10 min then resuspended in DMEM media supplemented with 10% fetal bovine serum. Cells were then incubated on a 24-well plate overnight prior to experimentation.

Statistics

All results are provided as means ± standard errors of the mean. All statistical analysis was performed using GraphPad Prism (San Diego, CA). Differences between the two groups over time (indicated in the relevant figure legends) were determined by a two-way analysis of variance (ANOVA) for repeated measures. For comparison between two independent groups, a Student's *t*-test was utilized. Significance was accepted at a P value of <0.05.

Supplementary Material

Refer to Web version on PubMed Central for supplementary material.

Acknowledgments

We kindly thank J. Song and for technical assistance, in addition to the rest of the Scherer laboratory for helpful discussions. We would also like to thank R. Hammer and the UTSW Transgenic Core Facility for the generation of mouse models as well as the UTSW Metabolic Core Facility, in particular Aktar Ali for help in the phenotypic characterization of the mice. The authors were supported by US National Institutes of Health grants R01-DK55758, R01-DK099110 and P01DK088761 (to P.E.S.). C.M.K. was supported by a fellowship from the Juvenile Diabetes Foundation (JDRF 3-2008-130). J.P. was supported in part by the 2014 research fund (1.130088.01) of UNIST (Ulsan National Institute of Science and Technology).

Author Manuscript Author Manuscript Author Manuscript Author Manuscript

References

1. Zimmet P, Alberti KG, Shaw J. Global and societal implications of the diabetes epidemic. Nature. 2001; 414:782–787.10.1038/414782a [PubMed: 11742409]
2. Axen KV, Dikeakos A, Sclafani A. High dietary fat promotes syndrome X in nonobese rats. The Journal of nutrition. 2003; 133:2244–2249. [PubMed: 12840187]
3. Bessesen DH. The role of carbohydrates in insulin resistance. The Journal of nutrition. 2001; 131:2782S–2786S. [PubMed: 11584106]
4. Storlien LH, Tapsell LC, Calvert GD. Diabetic diets--whither goest? Nutrition. 1998; 14:865–867. [PubMed: 9834930]
5. Virtue S, Vidal-Puig A. Adipose tissue expandability, lipotoxicity and the Metabolic Syndrome--an allostatic perspective. Biochimica et biophysica acta. 2010; 1801:338–349.10.1016/j.bbalip.2009.12.006 [PubMed: 20056169]
6. Hardy OT, Czech MP, Corvera S. What causes the insulin resistance underlying obesity? Current opinion in endocrinology, diabetes, and obesity. 2012; 19:81–87.10.1097/MED.0b013e3283514e13
7. Medina-Gomez G. Mitochondria and endocrine function of adipose tissue. Best practice & research. Clinical endocrinology & metabolism. 2012; 26:791–804.10.1016/j.beem.2012.06.002 [PubMed: 23168280]
8. Osellame LD, Blacker TS, Duchen MR. Cellular and molecular mechanisms of mitochondrial function. Best practice & research. Clinical endocrinology & metabolism. 2012; 26:711–723.10.1016/j.beem.2012.05.003 [PubMed: 23168274]
9. Enache I, et al. Skeletal muscle mitochondrial dysfunction precedes right ventricular impairment in experimental pulmonary hypertension. Molecular and cellular biochemistry. 2013; 373:161–170.10.1007/s11010-012-1485-6 [PubMed: 23099843]
10. Kim JA, Wei Y, Sowers JR. Role of mitochondrial dysfunction in insulin resistance. Circulation research. 2008; 102:401–414.10.1161/CIRCRESAHA.107.165472 [PubMed: 18309108]
11. McBride HM, Neuspiel M, Wasiak S. Mitochondria: more than just a powerhouse. Current biology: CB. 2006; 16:R551–560.10.1016/j.cub.2006.06.054 [PubMed: 16860735]
12. Fisher-Wellman KH, Neufer PD. Linking mitochondrial bioenergetics to insulin resistance via redox biology. Trends in endocrinology and metabolism: TEM. 2012; 23:142–153.10.1016/j.tem.2011.12.008 [PubMed: 22305519]
13. Kusminski CM, Scherer PE. Mitochondrial dysfunction in white adipose tissue. Trends in endocrinology and metabolism: TEM. 2012; 23:435–443.10.1016/j.tem.2012.06.004 [PubMed: 22784416]
14. De Pauw A, Tejerina S, Raes M, Keijer J, Arnould T. Mitochondrial (dys)function in adipocyte (de)differentiation and systemic metabolic alterations. The American journal of pathology. 2009; 175:927–939.10.2353/ajpath.2009.081155 [PubMed: 19700756]
15. Rossmeisl M, et al. Decreased fatty acid synthesis due to mitochondrial uncoupling in adipose tissue. FASEB journal: official publication of the Federation of American Societies for Experimental Biology. 2000; 14:1793–1800. [PubMed: 10973929]
16. Lowell BB, Shulman GI. Mitochondrial dysfunction and type 2 diabetes. Science. 2005; 307:384–387.10.1126/science.1104343 [PubMed: 15662004]
17. Rong JX, et al. Adipose mitochondrial biogenesis is suppressed in db/db and high-fat diet-fed mice and improved by rosiglitazone. Diabetes. 2007; 56:1751–1760.10.2337/db06-1135 [PubMed: 17456854]
18. Kusminski CM, et al. MitoNEET-driven alterations in adipocyte mitochondrial activity reveal a crucial adaptive process that preserves insulin sensitivity in obesity. Nature medicine. 2012; 18:1539–1549.10.1038/nm.2899
19. Puigserver P, et al. A cold-inducible coactivator of nuclear receptors linked to adaptive thermogenesis. Cell. 1998; 92:829–839. [PubMed: 9529258]
20. Uldry M, et al. Complementary action of the PGC-1 coactivators in mitochondrial biogenesis and brown fat differentiation. Cell metabolism. 2006; 3:333–341.10.1016/j.cmet.2006.04.002 [PubMed: 16679291]

Author Manuscript Author Manuscript Author Manuscript Author Manuscript

21. Brondani LA, et al. The role of the uncoupling protein 1 (UCP1) on the development of obesity and type 2 diabetes mellitus. Arquivos brasileiros de endocrinologia e metabologia. 2012; 56:215–225. [PubMed: 22790465]
22. Cannon B, Nedergaard J. Metabolic consequences of the presence or absence of the thermogenic capacity of brown adipose tissue in mice (and probably in humans). Int J Obes (Lond). 2010; 34(Suppl 1):S7–16.10.1038/ijo.2010.177 [PubMed: 20935668]
23. Cannon B, Nedergaard J. Nonshivering thermogenesis and its adequate measurement in metabolic studies. The Journal of experimental biology. 2011; 214:242–253.10.1242/jeb.050989 [PubMed: 21177944]
24. Golozoubova V, et al. Depressed thermogenesis but competent brown adipose tissue recruitment in mice devoid of all hormone-binding thyroid hormone receptors. Mol Endocrinol. 2004; 18:384–401.10.1210/me.2003-0267 [PubMed: 14630998]
25. Porter WP, Kearney M. Size, shape, and the thermal niche of endotherms. Proceedings of the National Academy of Sciences of the United States of America. 2009; 106(Suppl 2):19666–19672.10.1073/pnas.0907321106 [PubMed: 19846790]
26. Greenberg AS, et al. Stimulation of lipolysis and hormone-sensitive lipase via the extracellular signal-regulated kinase pathway. The Journal of biological chemistry. 2001; 276:45456–45461.10.1074/jbc.M104436200 [PubMed: 11581251]
27. Shoelson SE, Lee J, Goldfine AB. Inflammation and insulin resistance. The Journal of clinical investigation. 2006; 116:1793–1801.10.1172/JCI29069 [PubMed: 16823477]
28. Osborn O, Olefsky JM. The cellular and signaling networks linking the immune system and metabolism in disease. Nature medicine. 2012; 18:363–374.10.1038/nm.2627
29. Sun K, Kusminski CM, Scherer PE. Adipose tissue remodeling and obesity. The Journal of clinical investigation. 2011; 121:2094–2101.10.1172/JCI45887 [PubMed: 21633177]
30. Neels JG, Olefsky JM. Inflamed fat: what starts the fire? The Journal of clinical investigation. 2006; 116:33–35.10.1172/JCI27280 [PubMed: 16395402]
31. Xu H, et al. Chronic inflammation in fat plays a crucial role in the development of obesity-related insulin resistance. J Clin Invest. 2003; 112:1821–1830. [PubMed: 14679177]
32. Weisberg SP, et al. Obesity is associated with macrophage accumulation in adipose tissue. The Journal of clinical investigation. 2003; 112:1796–1808.10.1172/JCI19246 [PubMed: 14679176]
33. Lumeng CN, Bodzin JL, Saltiel AR. Obesity induces a phenotypic switch in adipose tissue macrophage polarization. The Journal of clinical investigation. 2007; 117:175–184.10.1172/JCI29881 [PubMed: 17200717]
34. Cipolletta D, Kolodin D, Benoist C, Mathis D. Tissular T(regs): a unique population of adipose-tissue-resident Foxp3+CD4+ T cells that impacts organismal metabolism. Seminars in immunology. 2011; 23:431–437.10.1016/j.smim.2011.06.002 [PubMed: 21724410]
35. Cipolletta D, et al. PPAR-gamma is a major driver of the accumulation and phenotype of adipose tissue Treg cells. Nature. 2012; 486:549–553.10.1038/nature11132 [PubMed: 22722857]
36. Strissel KJ, et al. T-cell recruitment and Th1 polarization in adipose tissue during diet-induced obesity in C57BL/6 mice. Obesity (Silver Spring). 2010; 18:1918–1925.10.1038/oby.2010.1 [PubMed: 20111012]
37. Lumeng CN, Maillard I, Saltiel AR. T-ing up inflammation in fat. Nature medicine. 2009; 15:846–847.10.1038/nm0809-846
38. Harford KA, Reynolds CM, McGillicuddy FC, Roche HM. Fats, inflammation and insulin resistance: insights to the role of macrophage and T-cell accumulation in adipose tissue. Proc Nutr Soc. 2011; 70:408–417.10.1017/S0029665111000565 [PubMed: 21835098]
39. Ji Y, et al. Short term high fat diet challenge promotes alternative macrophage polarization in adipose tissue via natural killer T cells and interleukin-4. The Journal of biological chemistry. 2012; 287:24378–24386.10.1074/jbc.M112.371807 [PubMed: 22645141]
40. Eller K, et al. Potential role of regulatory T cells in reversing obesity-linked insulin resistance and diabetic nephropathy. Diabetes. 2011; 60:2954–2962.10.2337/db11-0358 [PubMed: 21911743]
41. Ilan Y, et al. Induction of regulatory T cells decreases adipose inflammation and alleviates insulin resistance in ob/ob mice. Proceedings of the National Academy of Sciences of the United States of America. 2010; 107:9765–9770.10.1073/pnas.0908771107 [PubMed: 20445103]

Author Manuscript Author Manuscript Author Manuscript Author Manuscript

42. Kim KY, Jeong HJ, Kim HM. The role of T-bet in obesity: lack of T-bet causes obesity in male mice. The Journal of nutritional biochemistry. 2013; 24:240–247.10.1016/j.jnutbio.2012.05.010 [PubMed: 22901686]
43. Feng B, Zhang T, Xu H. Human adipose dynamics and metabolic health. Annals of the New York Academy of Sciences. 2013; 1281:160–177.10.1111/nyas.12009 [PubMed: 23317303]
44. Silva JE. Thermogenic mechanisms and their hormonal regulation. Physiological reviews. 2006; 86:435–464.10.1152/physrev.00009.2005 [PubMed: 16601266]
45. Klingenspor M, Herzig S, Pfeifer A. Brown fat develops a brite future. Obesity facts. 2012; 5:890–896.10.1159/000346337 [PubMed: 23296106]
46. Si Y, Palani S, Jayaraman A, Lee K. Effects of forced uncoupling protein 1 expression in 3T3-L1 cells on mitochondrial function and lipid metabolism. Journal of lipid research. 2007; 48:826–836.10.1194/jlr.M600343-JLR200 [PubMed: 17202129]
47. Enerback S, et al. Mice lacking mitochondrial uncoupling protein are cold-sensitive but not obese. Nature. 1997; 387:90–94.10.1038/387090a0 [PubMed: 9139827]
48. Feldmann HM, Golozoubova V, Cannon B, Nedergaard J. UCP1 ablation induces obesity and abolishes diet-induced thermogenesis in mice exempt from thermal stress by living at thermoneutrality. Cell metabolism. 2009; 9:203–209.10.1016/j.cmet.2008.12.014 [PubMed: 19187776]
49. McLaughlin T, Lamendola C, Liu A, Abbasi F. Preferential fat deposition in subcutaneous versus visceral depots is associated with insulin sensitivity. The Journal of clinical endocrinology and metabolism. 2011; 96:E1756–1760.10.1210/jc.2011-0615 [PubMed: 21865361]
50. Karelis AD, et al. The metabolically healthy but obese individual presents a favorable inflammation profile. The Journal of clinical endocrinology and metabolism. 2005; 90:4145–4150.10.1210/jc.2005-0482 [PubMed: 15855252]
51. Sims EA. Are there persons who are obese, but metabolically healthy? Metabolism: clinical and experimental. 2001; 50:1499–1504.10.1053/meta.2001.27213 [PubMed: 11735101]
52. Karelis AD, St-Pierre DH, Conus F, Rabasa-Lhoret R, Poehlman ET. Metabolic and body composition factors in subgroups of obesity: what do we know? The Journal of clinical endocrinology and metabolism. 2004; 89:2569–2575.10.1210/jc.2004-0165 [PubMed: 15181025]
53. Wang QA, Tao C, Gupta RK, Scherer PE. Tracking adipogenesis during white adipose tissue development, expansion and regeneration. Nature medicine. 2013; 19:1338–1344.10.1038/nm.3324
54. Hotamisligil GS. Inflammation and metabolic disorders. Nature. 2006; 444:860–867.10.1038/nature05485 [PubMed: 17167474]
55. Christiaens V, Lijnen HR. Angiogenesis and development of adipose tissue. Molecular and cellular endocrinology. 2010; 318:2–9.10.1016/j.mce.2009.08.006 [PubMed: 19686803]
56. Sun K, et al. Dichotomous effects of VEGF-A on adipose tissue dysfunction. Proceedings of the National Academy of Sciences of the United States of America. 2012; 109:5874–5879.10.1073/pnas.1200447109 [PubMed: 22451920]
57. Sung HK, et al. Adipose vascular endothelial growth factor regulates metabolic homeostasis through angiogenesis. Cell metabolism. 2013; 17:61–72.10.1016/j.cmet.2012.12.010 [PubMed: 23312284]
58. Khan T, et al. Metabolic dysregulation and adipose tissue fibrosis: role of collagen VI. Molecular and cellular biology. 2009; 29:1575–1591.10.1128/MCB.01300-08 [PubMed: 19114551]
59. Divoux A, et al. Fibrosis in human adipose tissue: composition, distribution, and link with lipid metabolism and fat mass loss. Diabetes. 2010; 59:2817–2825.10.2337/db10-0585 [PubMed: 20713683]
60. Strissel KJ, et al. Adipocyte death, adipose tissue remodeling, and obesity complications. Diabetes. 2007; 56:2910–2918.10.2337/db07-0767 [PubMed: 17848624]
61. Kim JY, et al. Obesity-associated improvements in metabolic profile through expansion of adipose tissue. The Journal of clinical investigation. 2007; 117:2621–2637.10.1172/JCI31021 [PubMed: 17717599]

Author Manuscript Author Manuscript Author Manuscript Author Manuscript

62. Livak KJ, Schmittgen TD. Analysis of relative gene expression data using real-time quantitative PCR and the 2(−Delta Delta C(T)) Method. Methods. 2001; 25:402–408.10.1006/meth.2001.1262 [PubMed: 11846609]

Author Manuscript Author Manuscript Author Manuscript Author Manuscript

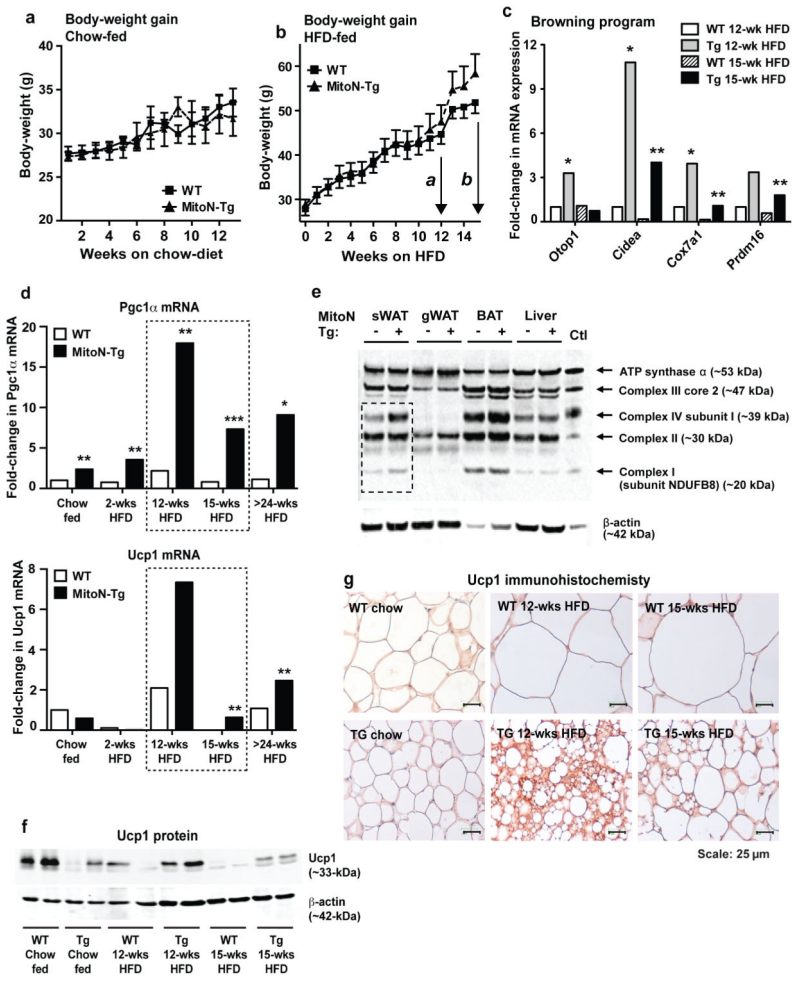

Figure 1. *MitoN-Tg* mice exhibit increased body-weight gain specifically at week-15 of HFD feeding due to a downregulation in the browning signature program

Body-weight gain in FVB wild-type (WT) mice and mitoNEET transgenic (*MitoN-Tg*) mice during (**a**) chow-diet feeding or (**b**) high-fat diet (HFD) feeding. In Fig. 1b, arrow a and arrow b correspond to the 12-week and 15-weeks stages of HFD feeding that microarray analysis was performed for, respectively. (**c**) Real-time qPCR confirmatory data of key brown adipose tissue (BAT)-marker genes, reflective of a browning signature program, identified from Illumina microarray profiling (*Otop1*, *Cidea*, *Cox7a1* and *Prdm16*) in sWAT derived from WT and *MitoN-Tg* mice fed HFD for either 12-weeks or 15-weeks. Data represents fold-change in gene expression when compared with WT sWAT under chow-fed conditions (n = 5 per group). (**d**) *Pgc1α* and *Ucp1* gene expression levels in WT sWAT and *MitoN-Tg* sWAT derived from mice that were fed a chow-diet, or HFD for 2-weeks, 12-weeks, 15-weeks or >24-weeks. Data represents fold-change in gene expression when compared with WT sWAT under chow-fed conditions (n = 5 per group). (**e**) Western blot of complex I (subunit NDUFB8), complex II, complex III (core 2), complex IV (subunit I) and ATP synthase α of the mitochondrial electron transport chain in WT and MitoN-Tg sWAT, gWAT, BAT and liver tissues (top panel). The lower panel shows β-actin expression levels. (**f**) Immunoblots showing Ucp1 protein expression (upper panel) and β-actin expression

Author Manuscript Author Manuscript Author Manuscript Author Manuscript

levels (lower panel), in addition to (**g**) Ucp1 immunohistochemistry (IHC) on WT sWAT and *MitoN-Tg* sWAT from mice that were fed a chow-diet, or HFD for 12-weeks or 15-weeks (n = 5 per group). All IHC images were obtained at 40X-magnification. Scale bar, 25 μm. Student's *t*-test, **P*<0.05; ***P*<0.01.

Author Manuscript Author Manuscript Author Manuscript Author Manuscript

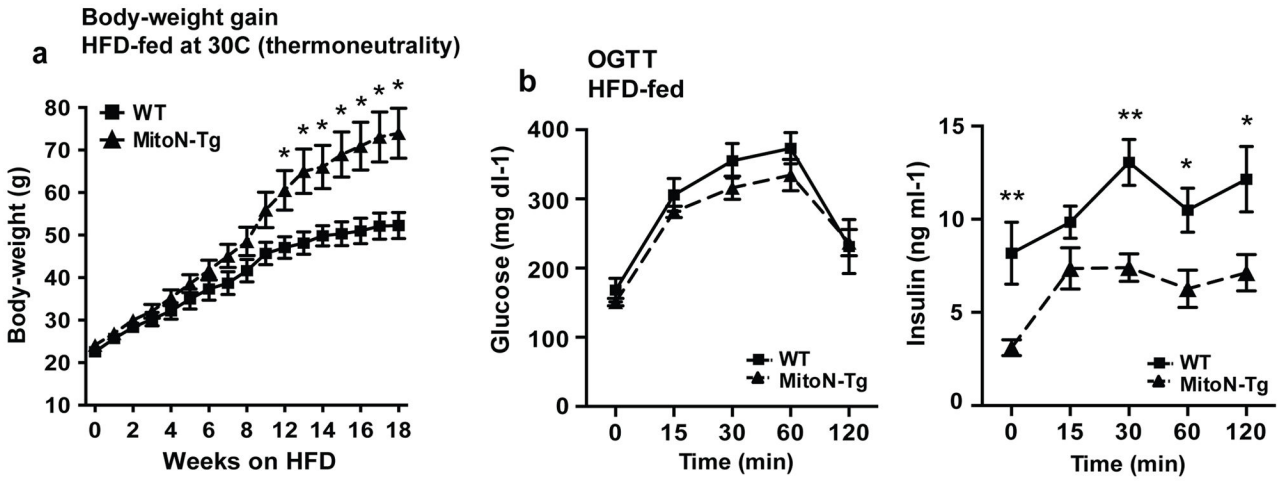

Figure 2. Thermoneutrality promotes a faster rate of WAT expansion in *MitoN-Tg* during HFD feeding

(a) Body-weight gain in male FVB WT and *MitoN-Tg* mice during HFD feeding under thermoneutral conditions (approximately 30°C). **(b)** Glucose values (left) and insulin values (right) from an oral glucose tolerance test (OGTT) performed on WT versus *MitoN-Tg* following 18-weeks of HFD feeding under thermoneutrality. Data represents mean ± s.e.m (n = 7 per group). Student's *t*-test, **P*<0.05; ***P*<0.01.

Author Manuscript
Author Manuscript
Author Manuscript
Author Manuscript

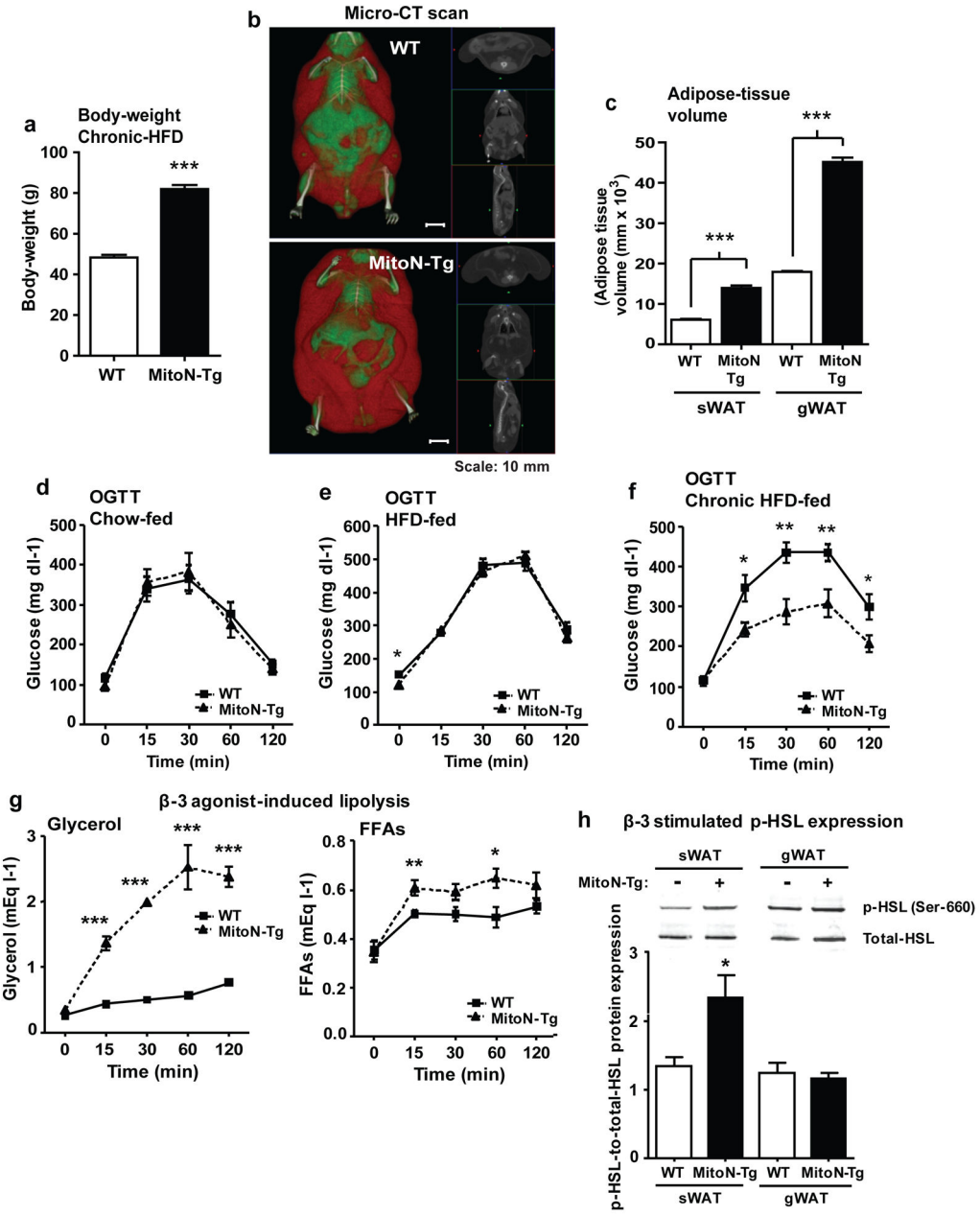

Author Manuscript Author Manuscript Author Manuscript Author Manuscript

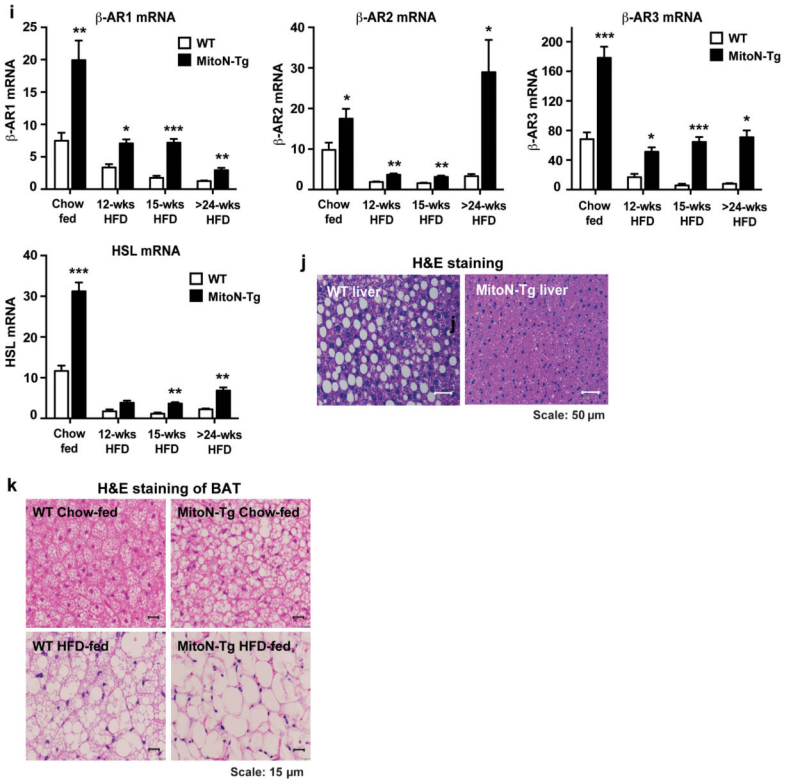

Figure 3. During chronic HFD feeding, *MitoN-Tg* mice exhibit improved insulin-sensitivity

(**a**) Body-weights of WT mice and *MitoN-Tg* mice following chronic (>15-weeks) HFD feeding (n = 5 per group). (**b**) A representative whole-body micro-CT scan of a chronic HFD-fed WT mouse (top) and a MitoN-Tg mouse (bottom). Scale bar, 10 mm. (**c**) sWAT and gWAT volume (mm × 10^3) (as determined by micro-CT scanning), following >15-weeks of chronic HFD feeding of WT mice and *MitoN-Tg* mice (n = 5 per group). An oral glucose tolerance test (OGTT) (2.5 g kg^{-1} bodyweight; single gavage) on FVB WT mice and *MitoN-Tg* mice following (**d**) chow-diet feeding, (**e**) 12-weeks of HFD-feeding or, (**f**) chronic (>15-weeks) HFD feeding (n = 5 per group). (**g**) Glycerol levels (left) and FFA levels (right) following a β-3 adrenergic agonist sensitivity test (1 mg kg^{-1} CL316, 243 i.p., single injection; n = 5 per group) of WT mice and *MitoN-Tg* mice that underwent chronic (>15-weeks) HFD-feeding. (**h**) Representative immunoblots showing β-3 stimulated (1 mg kg^{-1} CL316, 243 i.p., single injection) phospho-HSL (p-HSL) (Serine (Ser)-660) (top panel) and total-HSL (bottom panel) protein expression levels in WT and *MitoN-Tg* sWAT and gWAT fat-pads. Bar graphs show the calculated ratio of p-HSL-to-total-HSL protein expression levels in in WT and *MitoN-Tg* sWAT and gWAT fat-pads (n = 4 per group). (**i**) Gene expression levels of β-adrenergic receptor 1 *(β-AR1*), *β-AR2* and *β-AR3*, in addition to hormone sensitive lipase (HSL) in chow-fed, 12-week HFD-fed, 15-week HFD-fed and chronic (>24-weeks HFD-fed) WT versus *MitoN-Tg* sWAT. Data represents mean ± s.e.m (n = 5 per group). Student's *t*-test, **P*<0.05; ***P*<0.01; ****P*<0.001. **(j)** Representative H&E staining of chronic HFD-fed WT and *MitoN-Tg* liver tissues. All images were taken at 20X-magnification. Scale bar, 50 μm. **(k)** Representative H&E staining of BAT derived

from WT mice and *MitoN-Tg* mice that were chow-fed (top panel) or chronic-HFD fed (bottom panel). Scale bar, 15 μm.

Author Manuscript Author Manuscript Author Manuscript Author Manuscript

Author Manuscript
Author Manuscript
Author Manuscript
Author Manuscript

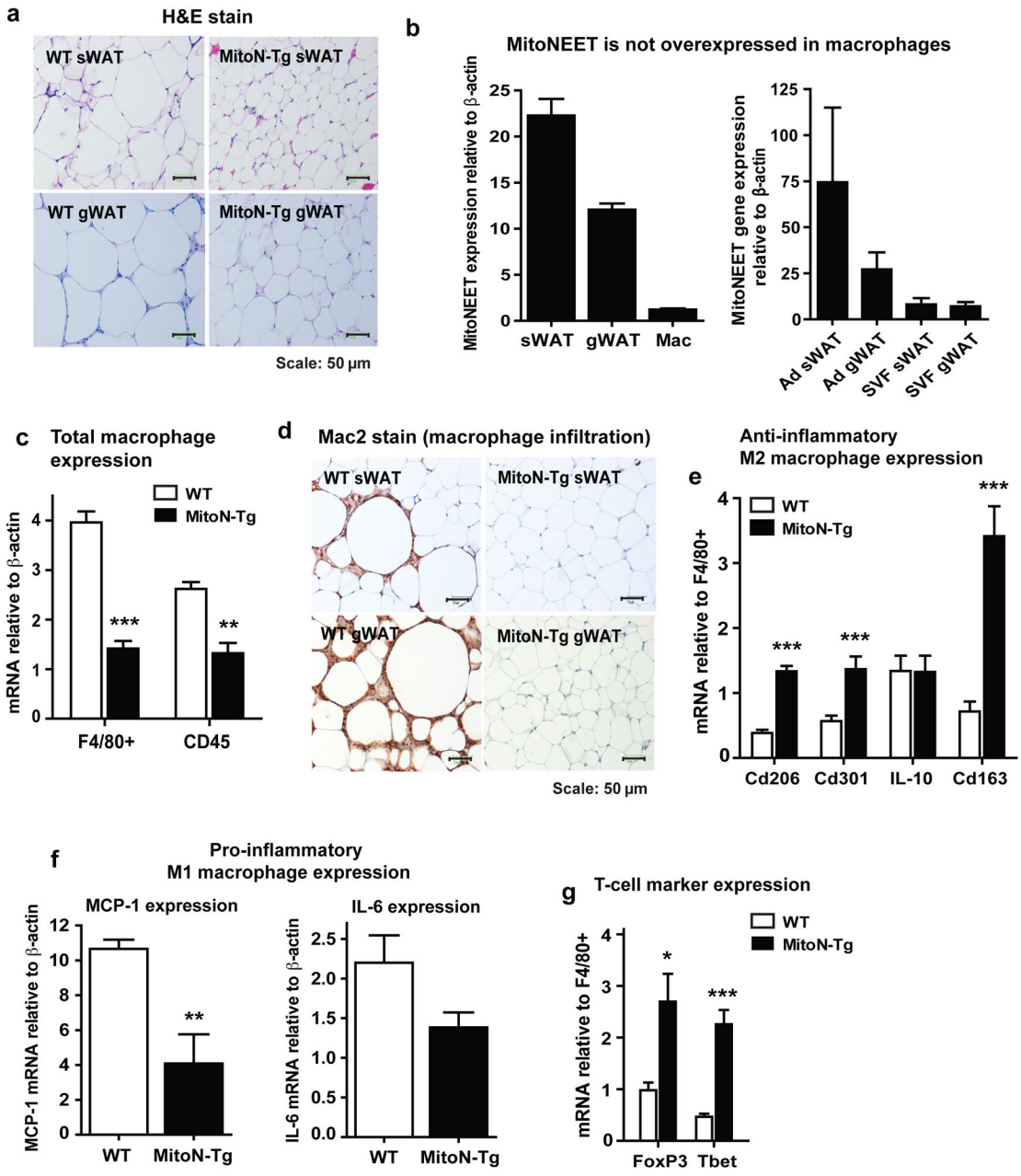

Figure 4. MitoNEET promotes an M2 anti-inflammatory phenotype in sWAT

(**a**) Representative H&E staining of chronic (>15-weeks) HFD-fed WT and *MitoN-Tg* sWAT (top panel) and gWAT (bottom panel). All images were obtained at 20X-magnification. Scale bar, 50 μm. (**b**) MitoNEET gene expression (relative to β-actin) in sWAT, gWAT and isolated macrophages (Mac) (n = 5 per group) (left panel), in addition to adipocyte (Ad) fractions and stromal vascular fractions (SVF) derived from unchallenged FVB WT and *MitoN-Tg* sWAT and gWAT (right panel) (n = 5 per group). (**c**) Total macrophage gene expression in WT and *MitoN-Tg* sWAT following chronic HFD feeding (n = 5 per group). (**d**) Representative images from Mac2 IHC staining of chronic HFD-fed WT and *MitoN-Tg* sWAT and gWAT. All images were taken at 20X-magnification. Scale bar,

Author Manuscript Author Manuscript Author Manuscript Author Manuscript

50 μm. (**e**) Anti-inflammatory M2 marker gene expression levels relative to *F4/80*$^+$ (*Cd206*, *Cd301*, *IL-10* and *Cd163*) in chronic HFD-fed WT and *MitoN-Tg* sWAT. Data represents mean ± s.e.m (n = 5 per group). (**f**) Pro-inflammatory M1 marker gene expression levels, relative to *F4/80*$^+$ (*Mcp-1* and *IL-6*) in chronic HFD-fed WT and *MitoN-Tg* sWAT (n = 5 per group). (**g**) T-cell marker gene expression levels, relative to *F4/80*$^+$ (*FoxP3* and *Tbet*) in chronic HFD-fed WT and *MitoN-Tg* sWAT. Data represents mean ± s.e.m (n = 5 per group). Student's *t*-test, **P*<0.05; ***P*<0.01; ****P*<0.001.

Author Manuscript Author Manuscript Author Manuscript Author Manuscript

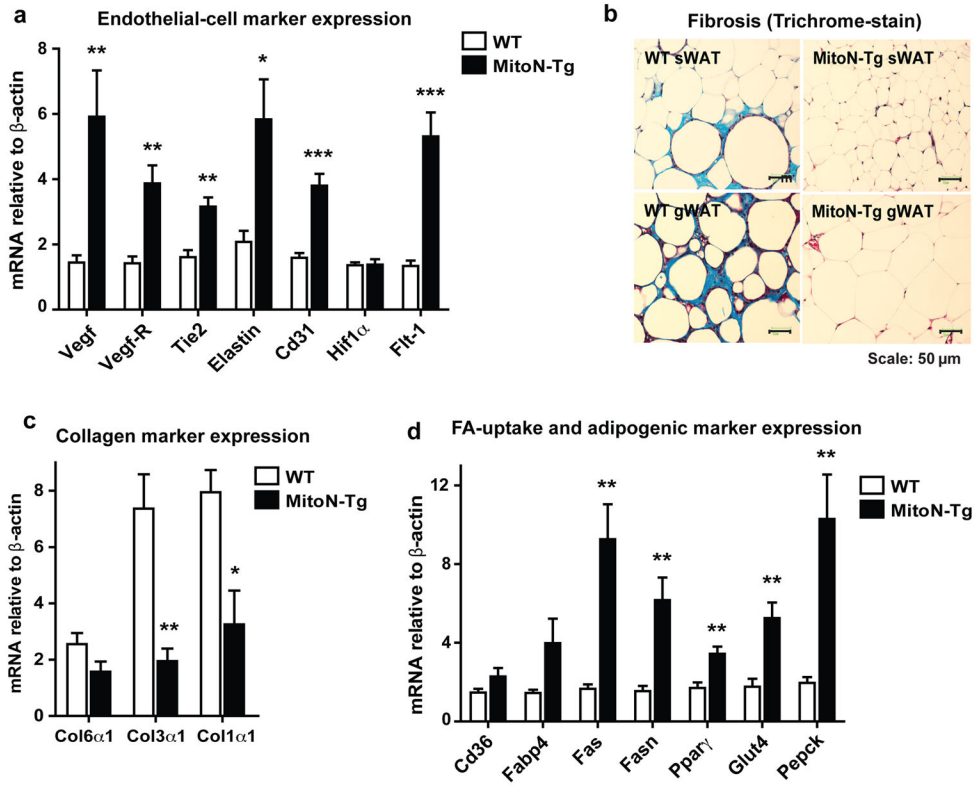

Figure 5. MitoNEET promotes healthy WAT expansion during HFD-feeding through stimulation of angiogenesis and reduction of collagens

(**a**) Endothelial cell marker gene expression levels relative to β-actin (*Vegf*, *Vegf-R*, *Tie2*, *Elastin*, *Cd31*, *Hif1α* and *Flt-1*) in chronic HFD-fed WT and *MitoN-Tg* sWAT. Data represents mean ± s.e.m (n = 5 per group). (**b**) Representative images of Trichrome stained sWAT and gWAT derived from chronic HFD-fed WT mice and *MitoN-Tg* mice; reflecting the degree of WAT fibrosis. Scale bar, 50 μm. (**c**) Collagen marker gene expression levels relative to β-actin (*Col6α1*, *Col3α1* and *Col1α1*) in chronic HFD-fed WT and *MitoN-Tg* sWAT (n = 5 per group). (**d**) Fatty acid (FA)-uptake, adipogenesis and glucose-uptake marker gene expression levels relative to β-actin (*Cd36*, *Fabp4*, *Fas*, *Fasn*, *Pparγ*, *Glut4* and *Pepck*) in chronic HFD-fed WT and *MitoN-Tg* sWAT. Data represents mean ± s.e.m (n = 5 per group). Student's *t*-test, **P*<0.05; ***P*<0.01; ****P*<0.001.

Author Manuscript Author Manuscript Author Manuscript Author Manuscript

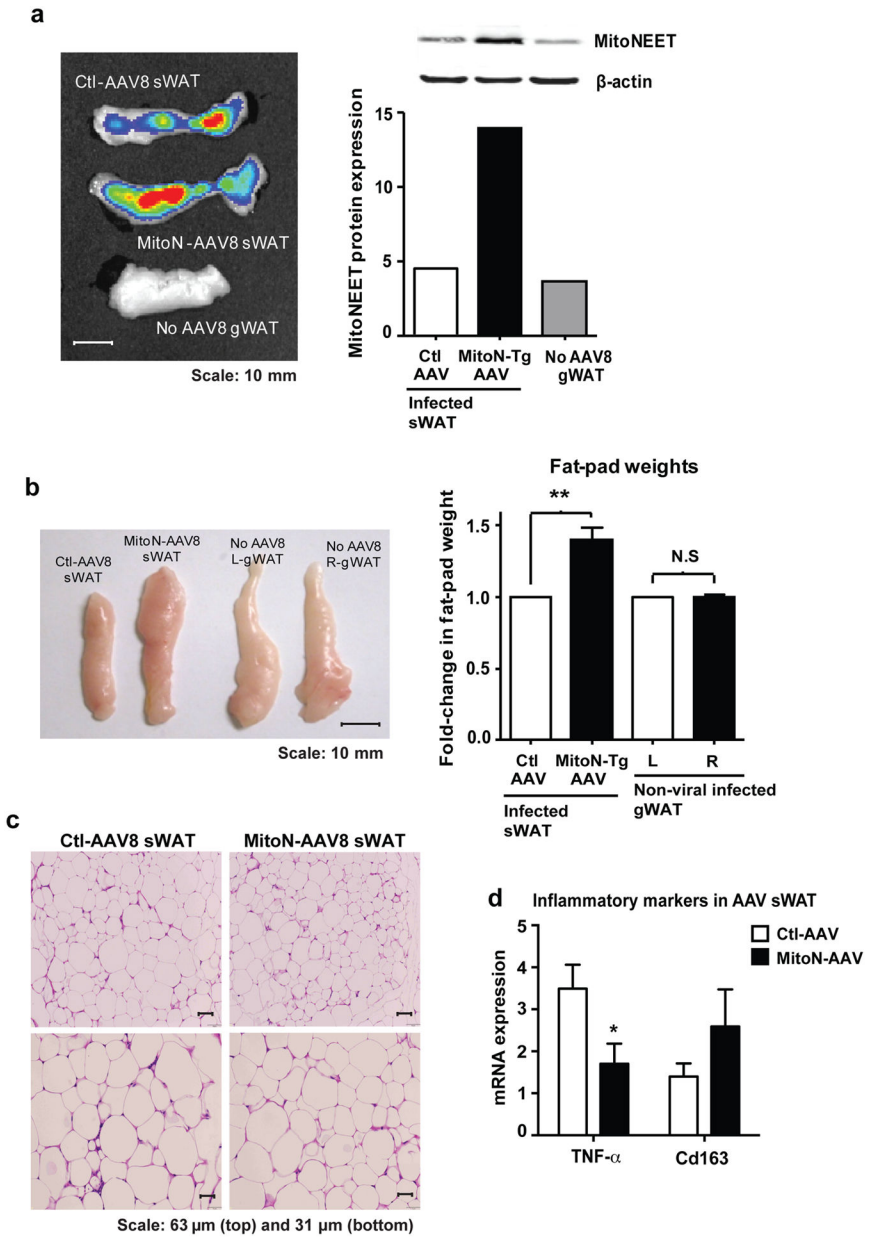

Figure 6. Adenoviral-mediated overexpression of mitoNEET promotes AT expansion

(**a**) Epi-fluorescence scan (left panel) showing GFP signal (radiant efficiency ([p/sec/cm^2/sr]/μW/cm^2) (viral-infection) and confirmation of mitoNEET protein overexpression in sWAT following viral-injection (right panel). Scale bar, 10 mm. (**b**) A representative photograph (left panel) following direct injection of control-virus (Ctl-AAV8-eGFP) or mitoNEET-virus (MitoN-AAV8-IRES-eGFP) (5×10^{11} PFU total sWAT injection) into left and right sWAT fat-pads of 12-week old WT FVB mice HFD-fed for 4-weeks, respectively. Scale bar, 10 mm. Non-infected left (L) and right (R) gWAT fat-pads serve as additional internal controls. Fold-change in L versus R sWAT (control or mitoNEET viral-infected, respectively) and L versus R gWAT (non-viral-infected) fat-pad weights, following HFD-feeding (4-weeks) of WT mice (right panel) (n = 6 per group).

Author Manuscript Author Manuscript Author Manuscript Author Manuscript

Student's *t*-test, ***P*<0.01. **(c)** Representative H&E stained images of Ctl-AAV8 (left) and MitoN-AAV8 (right) infected sWAT. Scale bar, 63 μm (top panel) and 31 μm (bottom panel). **(d)** TNFα and Cd163 gene expression levels in Ctl-AAV versus MitoN-AAV8 sWAT. Data represents mean ± s.e.m (n = 4 per group). Student's *t*-test, **P*<0.05.

Author Manuscript

Author Manuscript

Author Manuscript

Author Manuscript

Table 1

Key microarray genes that are *upregulated* between 12–15 weeks HFD feeding

Top differentially regulated pathways and genes by microarray analyses that are *upregulated* specifically between *MitoN-Tg* sWAT from 12-weeks HFD feeding versus *MitoN-Tg* sWAT from 15-weeks of HFD feeding, which are *unaltered* in WT sWAT within the same timeframe. Inclusion criteria entailed genes that are upregulated more than 1.4-fold in *MitoN-Tg* sWAT between weeks-12 and weeks-15 HFD, exhibit an absolute value of over 500 in abundance and, are not profoundly altered (or regulated in the opposite direction to *MitoN-Tg*) in WT sWAT, within the same HFD feeding timeframe. Gene abbreviations, definitions, in addition to fold-alterations between *MitoN-Tg* sWAT week-12 HFD *versus* week-15 HFD groups are indicated (n = 5 per group).

Gene	Gene definition	Fold ↑	Function in metabolism
11-βHSD1	11-β hydroxysteroid dehydrogenase type 1	1.7-fold	Generates glucocorticoids in adipose tissue
Egr1	Early growth response protein 1	1.7-fold	Downstream target of Fgf21
Sema5a	Semaphorin 5a	1.6-fold	Promotes angiogenesis
Col16a1	Collagen α-1 (XVI) chain	1.4-fold	Maintains the integrity of the extracellular matrix
Rarres2	Retinoic acid receptor responder protein 2	1.4-fold	Pparγ target gene; role in adipocyte differentiation

Author Manuscript

Author Manuscript

Author Manuscript

Author Manuscript

Table 2

Key microarray genes that are *downregulated* between 12–15 weeks HFD feeding

Top genes and clusters identified by microarray analysis that are *downregulated* specifically between *MitoN-Tg* sWAT from 12-weeks HFD feeding versus *MitoN-Tg* sWAT from 15-weeks of HFD feeding, which are *unaltered* in WT sWAT within the same timeframe. Inclusion criteria entailed genes that are downregulated more than 1.4-fold in *MitoN-Tg* sWAT between weeks-12 and weeks-15 HFD, exhibit an absolute value of over 500 in abundance and, are not profoundly altered (or regulated in the opposite direction to *MitoN-Tg*) in WT sWAT, within the same HFD feeding timeframe. Gene abbreviations, definitions, in addition to fold-alterations between *MitoN-Tg* sWAT week-12 HFD versus week-15 HFD groups are indicated (n = 5 per group).

Pathway Gene	Gene definition	Fold ↓	Function in metabolism
Browning			
Otop1	Otopetrin 1	2.9-fold	BAT-selective thermogenic gene
Cidea	Cell death activator CIDE-A	1.9-fold	Promotes thermogenesis and lipolysis
Ucp1	Uncoupling protein 1 (thermogenin)	4.0-fold	Heat generation, non-shivering thermogenesis
Cox7a1	Cytochrome c oxidase polypeptide 7A1	2.4-fold	Mitochondrial brown-adipocyte indicator gene
Cox8b	Cytochrome c oxidase subunit V111b	2.3-fold	Mitochondrial brown-adipocyte indicator gene
β-oxidation			
Acadvl	Acyl-CoA dehydrogenase	2.1-fold	Catalyzes the first step of β-oxidation
Cyp2e1	Cytochrome P450 2E1	1.9-fold	β-oxidation of unsaturated fatty acids; promotes ROS
Cpt2	Carnitine palmitoyltransferase 2	1.9-fold	Inner mitochondrial membrane β-oxidation enzyme
Acaa2	Acetyl-Coenzyme A acyltransferase 2	1.7-fold	Catalyzes the last step of β-oxidation
Slc25a20	Acylcarnitine translocase (solute carrier 25)	1.7-fold	Transports carnitine-FAs to mitochondria for oxidation
Aco2	Aconitase 2	1.6-fold	Mitochondrial TCA cycle enzyme
Decr1	2,4-dienoyl CoA reductase 1	1.6-fold	Enzyme of β-oxidation of fatty enoyl-CoA esters
Etfb	Electron-transfer-flavoprotein	1.6-fold	Shuttles electrons to mitochondrial respiratory chain
Gpd1	Glycerol-3-phosphate dehydrogenase	1.5-fold	Contributor of electrons to the respiratory chain

Author Manuscript

Author Manuscript

Author Manuscript

Author Manuscript

Table 3

Primer sequences

A list of RT-PCR primer sequences of utilized to assess sWAT derived from WT mice versus *MitoN-Tg* mice.

Gene	Forward primer	Reverse primer
β-*actin*	TACCACAGGCATTGTGATGG	TTTGATGTCACGCACGATTT
MitoNEET	ATGCCTTCGACATGGAGGATCT	TCGTTGTGCTTTATGTGAGCCC
Pgc1α	TCCTCACACCAAACCCACAGAA	TTGGCTTGAGCATGTTGCGA
Ucp1	GTGAAGGTCAGAATGCAAGC	AGGGCCCCCTTCATGAGGTC
F4/80^{+}	CTTTGGCTATGGGCTTCCAGTC	GCAAGGAGGACAGAGTTTATCGTG
Cd206	TGTGGTGAGCTGAAAGGTGA	CAGGTGTGGGCGCAGGTAGT
Cd301	TGAGAAAGGCTTTAAGAACTGGG	GACCACCTGTAGTGATGTGGG
IL-10	GCTCTTACTGACTGGCATGAG	CGCAGCTCTAGGAGCATGTG
Cd163	TCCACACGTCCAGAACAGTC	CCTTGGAAACAGAGACAGGC
Mcp-1	ACTGAAGCCAGCTCTCTCTTCC	TTCCTTCTTGGGGTCAGCACAG
IL-6	CCAGAGATACAAAGAAATGATGG	ACTCCAGAAGACCAGAGGAAAT
FoxP3	TCAAGTACCACAATATGCGACC	CCATCGGATAAGGGTGGCA
Tbet	GCCAGGGAACCGCTTATATG	GACGATCATCTGGGTCACATTGT
Vegf-A	GGAGATCCTTCGAGGAGCACTT	GGCGATTTAGCAGCAGATATAAGAA
Vegf-R	TGCCTACCTCACCTGTTTCC	AAGGACCATCCCACTGTCTG
Tie2	AAGCAACCCAGCCTTTTCTC	TGAGCATTCTCCTTTGGAC
Elastin	TGGTATTGGTGGCATCGG	CCTTGGCTTTGACTCCTGTG
Cd31	ATGACCCAGCAACATTCACA	CGACAGGATGGAAATCAACAA
Hif1α	CAAGATCTCGGCGAAGCAA	GGTGAGCCTCATAACAGAAGCTTT
Flt-1	TGCCTACCTCACCTGTTTCC	AAGGACCATCCCACTGTCTG
Col6a1	GATGAGGGTGAAGTGGGAGA	CAGCACGAAGAGGATGTCAA
Col3a1	GGGTTTCCCTGGTCCTAAAG	CCTGGTTTCCCATTTTCTCC
Col1α1	GTGCTCCTGGTATTGCTGGT	AAGGACCATCCCACTGTCTG
Cd36	TGAGACTGGGACCATTGGTGAT	CCCAAGTAAGGCCATCTCTACCAT
Fabp4	GACGACAGGAAGGTGAAGAG	ACATTCCACCACCAGCTTGT
Fas	CCTGGATAGCATTCCGAACCT	AGCACATCTCGAAGGCTACACA
Fasn	AAGTTGCCCGAGTCAGAGAA	CGTCGAACTTGGAGAGATCC
Pparγ	TCAGAGGGACAAGGATTCATGA	CACCAAAGGGCTTCCGCAGGCT
Glut4	AAGATGGCCACGGAGAGAG	GTGGGTTGTGGCAGTGAGTC
Pepck	CGCAAGCTGAAGAAAATATGACAA	TCGATCCTGGCCACATCTC